Journal of Oral Biosciences 68 (2026) 100746

Contents lists available at ScienceDirect

Journal of Oral Biosciences

journal homepage: www.elsevier.com/locate/job

Oral SARS-CoV-2 inoculation leads to distinct viral distribution compared to nasal inoculation in a Syrian hamster model

Nao Gojo [a], Yu Usami [b,c,*], Katsutoshi Hirose [b,c], Satoru Toyosawa [b], Shintaro Shichinohe [d], Tokiko Watanabe [c,d,e], Chikako Ono [c,e,f], Tsuyoshi Inoue [c,g], Takayoshi Sakai [a,c,**]

[a] Department of Rehabilitation for Orofacial Disorders, The University of Osaka Graduate School of Dentistry, Yamadaoka 1-8, Suita, Osaka, 565-0871, Japan
[b] Department of Oral and Maxillofacial Pathology, The University of Osaka Graduate School of Dentistry, Yamadaoka 1-8, Suita, Osaka, 565-0871, Japan
[c] Center for Infectious Disease Education and Research (CiDER), The University of Osaka, Yamadaoka 1-10, Suita, Osaka, 565-0871, Japan
[d] Department of Molecular Virology, Research Institute for Microbial Disease, The University of Osaka, Yamadaoka 3-1, Suita, Osaka, 565-0871, Japan
[e] Center for Advanced Modalities and DDS (CAMaD), The University of Osaka, Yamadaoka 3-1, Suita, Osaka, 565-0871, Japan
[f] Laboratory of Virus Control, Research Institute for Microbial Diseases, The University of Osaka, Yamadaoka 3-1, Suita, Osaka, 565-0871, Japan
[g] Division of Advance Pharmaco-Science, Graduate School of Pharmaceutical Sciences, The University of Osaka, Yamadaoka 1-6, Suita, Osaka, 565-0871, Japan

ARTICLE INFO

Keywords:
SARS-CoV-2
COVID19
Infection
Salivary gland
Animal model

ABSTRACT

Objectives: The nose and mouth are the primary entry points for upper respiratory severe acute respiratory syndrome coronavirus 2 (SARS-CoV-2) infection; however, the influence of different entry routes on viral spread remains unclear. Oral and nasal infection routes in terms of viral distribution and presence of inflammation were compared.

Methods: Syrian hamsters were inoculated with SARS-CoV-2 via three routes: nasal inoculation (NI), simulating conventional upper respiratory infection; lingual (supra-lingual) inoculation (LI), simulating exposure during speaking and eating; and sublingual inoculation (SI), simulating exposure to the salivary glands. After three days, the lungs, submandibular glands, nasal turbinates, liver, and brain were examined histologically and immunohistochemically. To assess direct access to the lungs, India ink was administered via each route and analyzed after tissue clearing.

Results: NI resulted in infection in the nasal olfactory sensory epithelium of the nasal cavity and in the lungs. India ink studies suggest that the virus is likely to have infected the nasal mucosa first, followed by secondary infection of the lungs. LI resulted in marked infection of the submandibular glands with vascular involvement. In the LI and SI groups, no viral antigen was detected in the lungs; however, there was inflammation of the lungs, suggesting cytokine-mediated effects.

Conclusion: Different upper respiratory entry routes produced distinct pathological patterns. While nasal infection is well recognized, our findings indicate that salivary gland infection via SI may suggest an alternative pathway for systemic viral dissemination.

1. Introduction

Severe acute respiratory syndrome coronavirus 2 (SARS-CoV-2), the causative agent of coronavirus disease 2019 (COVID-19), emerged in late 2019 and led to profound public health and economic consequences [1]. The clinical presentation of COVID-19 is diverse, ranging from mild to severe illness, although most cases are mild and characterized by symptoms such as fever, cough, fatigue, and loss of taste or smell. Older adults and individuals with underlying conditions such as cardiovascular disease, hypertension, and chronic lung disease are at increased risk of developing severe respiratory illness and acute respiratory distress syndrome [2]. Acute respiratory distress syndrome is a frequent complication of severe coronavirus infections and is closely linked to the development of cytokine storms [3].

* Corresponding author. Department of Oral and Maxillofacial Pathology, The University of Osaka Graduate School of Dentistry, Yamadaoka 1-8, Suita, Osaka, 565-0871, Japan.
** Corresponding author. Department of Rehabilitation for Orofacial Disorders, The University of Osaka Graduate School of Dentistry, Yamadaoka 1-8, Suita, Osaka, 565-0871, Japan.
E-mail addresses: usami.yuu.dent@osaka-u.ac.jp (Y. Usami), sakai.takayoshi.dent@osaka-u.ac.jp (T. Sakai).

https://doi.org/10.1016/j.job.2026.100746
Received 16 October 2025; Received in revised form 16 January 2026; Accepted 19 January 2026
Available online 22 January 2026

Since the onset of the COVID-19 pandemic, numerous animal models have been developed to study the pathogenesis of the disease and to explore potential preventative and therapeutic strategies. These models provide valuable translational relevance, as they enable comprehensive evaluation of host–virus interactions and host immune responses, both of which play a critical role in the course of viral infection and disease progression [4]. SARS-CoV-2 is classified as an airborne pathogen that spreads through exposure to virus-containing aerosols, primarily via the upper respiratory tract, including the oral cavity. The oral cavity, which serves as the entry point to both the digestive and respiratory systems, plays an essential role in eating, speaking, and breathing [5–7]. Moreover, several tissues in the upper respiratory tract, including the tongue, nasal cavity, pharynx, and salivary glands, express coronavirus receptor proteins such as angiotensin-converting enzyme 2 [8–10]. Consequently, the nasal and oral cavities are considered major routes of SARS-CoV-2 infection. However, most animal studies have focused on the nasal route, with only a limited number investigating oral transmission [9,11–13].

In this study, we used a Syrian hamster model with three viral inoculation routes to examine whether the route of viral entry influences viral dissemination and the degree of inflammation: nasal inoculation (NI), representing conventional upper respiratory tract infection; lingual (supra-lingual) inoculation (LI), simulating exposure during speaking and eating; and sublingual inoculation (SI), designed to induce salivary gland infection.

2. Materials and methods

2.1. Viruses

The SARS-CoV-2 strain SARS-CoV-2/Hu/DP/Kng/19–020 (GenBank accession no. LC528232; lineage B) was kindly provided by the Kanagawa Prefectural Institute of Public Health. All experiments involving SARS-CoV-2 were conducted in a biosafety level 3 laboratory, in accordance with standard biosafety protocols approved by the Research Institute for Microbial Diseases at the University of Osaka.

2.2. Animals

Seven-week-old male Syrian hamsters were purchased from Japan SLC (Shizuoka, Japan). All animal experiments that did not involve the use of viruses were approved by the Committee on the Ethics of Animal Experiments of the University of Osaka Graduate School of Dentistry and were conducted in strict accordance with the guidelines of the University of Osaka Graduate School of Dentistry for the care and use of laboratory animals.

2.3. Viral inoculation

For viral inoculation, twelve hamsters were randomly divided into four groups of three: three viral inoculation groups (NI, LI, and SI) and one control group. Following inhalational isoflurane anesthesia (Viatris, Canonsburg, PA, USA), each hamster was inoculated with a total of 5×10^5 $TCID_{50}$/30 μL of SARS-CoV-2 culture supernatant using 20–100 μL pipettes (Thermo Fisher Scientific, Carlsbad, CA, USA) fitted with 200 μL tips (Thermo Fisher Scientific, Carlsbad, CA, USA). For NI, the pipette tip was carefully inserted into the right nostril, ensuring that no culture supernatant leaked into the mouth. For LI, the culture supernatant was applied over the tongue into the pharyngeal cavity. For SI, a pipette tip was inserted beneath the tongue to deliver the culture supernatant to the sublingual area (Fig. 1A). Three days after infection, the hamsters were euthanized and fixed by transcardial perfusion with 4 % paraformaldehyde phosphate buffer (Fujifilm Wako Pure Chemical Co., Tokyo, Japan). The lungs, head, submandibular glands (SMGs) and liver were removed and immersed in 4 % paraformaldehyde (Fujifilm Wako Pure Chemical Co., Osaka, Japan) for 24 h.

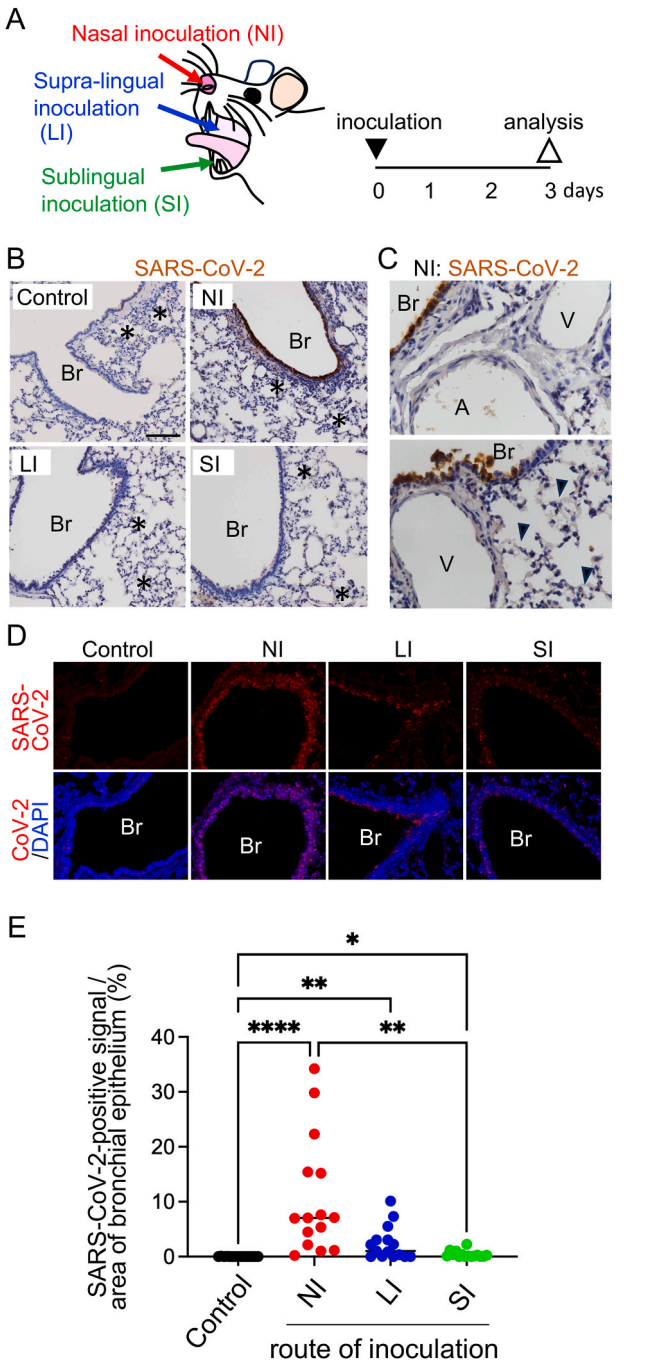

Fig. 1. Comparison of severe acute respiratory syndrome coronavirus 2 (SARS-CoV-2) localization and expression in the lungs across different inoculation routes.
(A) Schematic diagram of the inoculation routes. (B) Representative immunohistochemical images of SARS-CoV-2 in the lungs following the three inoculation routes. Scale bar: 100 μm. (C) Representative immunohistochemical images of the pulmonary artery and vein adjacent to the infected bronchiole. (D) Immunofluorescence images of hamster lungs after the three inoculation routes. Upper panels: SARS-CoV-2 (red); lower panels: merged images of SARS-CoV-2 and DAPI (blue). (E) Percentage of SARS-CoV-2-positive area in the lungs after each inoculation method. ****$p < 0.0001$; **$p < 0.01$; *$p < 0.05$. (B–D) Br: bronchiole; *: alveolar area; A: pulmonary artery; V: pulmonary vein; arrowhead: alveolar capillary. (B–E) Control: no virus; NI: nasal inoculation; LI: supra-lingual inoculation; SI: sublingual inoculation.

2.4. Tissue processing and histopathological analysis

After fixation, the head, lung, salivary glands, brain, and liver were processed and embedded in paraffin, and tissue sections were prepared for immunohistochemical and hematoxylin-eosin (HE) staining. Detailed procedures are provided in the Supplementary Materials and Methods.

2.5. Immunohistochemistry and immunofluorescence

For immunohistochemistry, tissue sections were incubated with either a rabbit anti-SARS-CoV-2 nucleoprotein antibody (Sino Biological, Beijing, China) or a rabbit anti-cleaved caspase 3 antibody (Cell Signaling Technology, Danvers, MA, USA). For immunofluorescence, sections were incubated overnight at 4 °C with a rabbit anti-CD45 antibody (Abcam, Cambridge, UK) alone or with a rabbit anti-SARS-CoV-2 antibody (Sino Biological) combined with a goat anti-olfactory marker protein antibody (Fujifilm Wako Pure Chemical Co.) or with a goat anti-CD31 antibody (R&D systems, Minneapolis, MN, U.S.A.). Nuclei were counterstained with DAPI (4′,6-diamidino-2-phenylindole). Detailed procedures are provided in the Supplementary Materials and Methods.

2.6. Evaluation of immunohistochemistry and immunofluorescence

SARS-CoV-2 expression in the bronchial epithelium, ductal epithelium of the SMG, and vessel wall of the SMG was analyzed by quantifying SARS-CoV-2-positive signals (pixels) within the area of each structure (μm^2). For immunofluorescence, regions of interest were captured from each specimen using a confocal laser microscope. The resulting images were analyzed with the ImageJ 1.53 software (National Institutes of Health, Bethesda, MD, USA [14]). Detailed procedures are provided in the Supplementary Materials and Methods. The number of evaluated areas was as follows: bronchial epithelium, five fields per animal; ductal epithelium of the SMG, 10 fields per animal; and vessel wall of the SMG, a total of 27 vessels across 10 fields per animal.

The numbers of CD45-positive and cleaved caspase 3-positive cells were also counted as described in the Supplementary Materials and Methods.

2.7. Analysis of bronchial inflammation

Bronchial inflammation was evaluated after HE staining using a light microscope, based on the established scoring system for influenza virus-associated lung inflammation [15,16]. Detailed procedures are provided in the Supplementary Materials and Methods.

2.8. India ink inoculation and tissue clearing

To assess whether the viral inoculum could reach the lungs, India ink was administered via three inoculation routes (NI, LI, and SI). Lung distribution of the ink was evaluated by stereomicroscopic imaging after tissue clearing, and quantitative analysis was performed using ImageJ [17,18]. Detailed procedures are provided in the Supplementary Materials and Methods.

2.9. Statistical analysis

Statistical analyses were performed using GraphPad Prism version 10 (GraphPad Software, San Diego, CA, USA). Data are presented as mean ± standard deviation. The Kruskal–Wallis one-way analysis of variance was used to assess differences among groups, and Dunn's post hoc test was applied for pairwise comparisons. A p-value of less than 0.05 was considered statistically significant.

3. Results

3.1. NI caused acute bronchitis with SARS-CoV-2 infection

To investigate how the route of viral transmission influences infection, we tested three upper respiratory inoculation routes in golden Syrian hamsters (Fig. 1A): NI, LI, and SI. Expression of coronavirus receptor proteins was confirmed by western blotting and immunohistochemistry (Supplementary Fig. S1) [19]. Because NI is known to induce lung infection, we confirmed the presence of SARS-CoV-2 in the lungs [12,20,21]. Immunohistochemistry using an anti-SARS-CoV-2 antibody revealed strong and widespread positive signals in the bronchiolar epithelium of the NI group, with weaker signals in the LI and SI groups (Fig. 1B). Although inflammatory cell infiltration was evident in the alveolar area, no viral signals were detected in any experimental group (asterisk in Fig. 1B). Viral signals were also absent in bronchial arteries, veins, and alveolar capillaries (Fig. 1C). Immunofluorescence was performed for quantitative assessment (Fig. 1D). The percentage of SARS-CoV-2-positive area was significantly higher in the NI group compared with the LI and SI groups (Fig. 1E).

3.2. LI and SI induced non-viral pneumonia and bronchitis

Because SARS-CoV-2 was undetectable in the lung of LI and SI group, we further evaluated and compare the severity of inflammation in lung tissue (Fig. 2A). Compare to control and SI groups, inflammation score, which reflects expansion and severity of inflammation, were significantly higher in NI group (Fig. 2B). Also, LI and SI group showed significant higher inflammatory score when compare to control group (Fig. 2B). Inflammatory cell infiltration in alveoli were assessed by measuring the number of CD45-positive cells (Fig. 2C). Among 3 experiment groups and control group, number of CD45-positive cells in the alveoli area was significantly higher in NI group, followed by SI and LI group (Fig. 2D). Because apoptosis of bronchial epithelium has been reported as one of characteristics during SARS-CoV-2 infection [22,23], bronchial apoptosis was assessed by evaluating the expression of Cleaved caspase-3 protein which serve as a key marker for apoptosis (Fig. 2E). The number of apoptotic cells was significantly higher in NI group when compare to other experiment group (Fig. 2F).

These results indicate that, among the three inoculation routes, NI caused the most severe SARS-CoV-2 infection and pulmonary inflammation, whereas the LI and SI routes induced non-viral pulmonary inflammation.

3.3. NI induced SARS-CoV-2 infection in the olfactory sensory epithelium (OSE)

Previous studies have visualized olfactory SARS-CoV-2 infection to explain loss of smell in patients with COVID-19 [24,25]. To determine whether all three inoculation routes induce infection in the nasal mucosa, frontal sections of the nasal cavity were histologically analyzed. HE staining revealed severe erosive inflammation of the nasal mucosa, including the OSE [26], in the NI group but not in the control, LI, or SI groups (Fig. 3A and B). Immunohistochemistry confirmed SARS-CoV-2 infection in the OSE of the NI group, but not in that of the control, LI, or SI groups (Fig. 3B). Pathological evaluation of the nasal cavity in the NI group also showed inflammatory cell infiltration with SARS-CoV-2, not only in abscesses within the turbinate passages but also in nasal glands adjacent to the OSE (Fig. 3C and D). Furthermore, immunohistochemistry using an anti-cleaved caspase 3 antibody revealed apoptotic cells in both the OSE and nasal glands (Fig. 3E). Immunofluorescence confirmed that olfactory marker protein-positive terminal dendritic trees of olfactory sensory neurons were embedded in the OSE, where viral signals were localized (Fig. 3F). Notably, viral signals were also detected within olfactory marker protein-positive olfactory sensory neurons (Fig. 3F, white arrowhead). These findings suggest that loss of

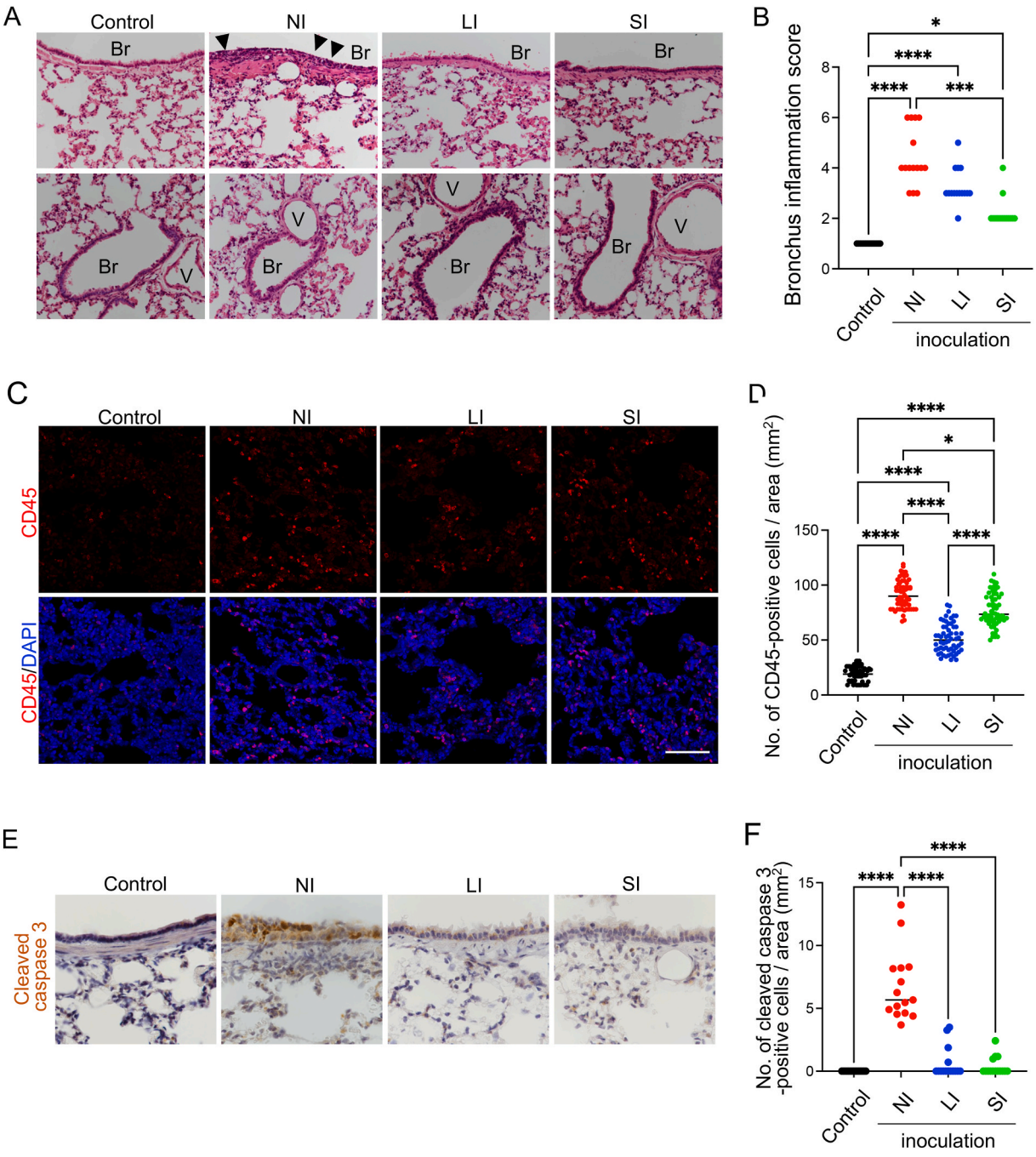

Fig. 2. Comparison of pulmonary inflammation across different inoculation routes.
(A) Representative histological images of lungs after severe acute respiratory syndrome coronavirus 2 (SARS-CoV-2) inoculation via the three routes. Br: bronchiole; V: pulmonary vein; arrowheads: acute bronchitis; *: alveolar area. (B) Bronchial inflammation scores. (C) Immunofluorescence images of the alveolar area stained with anti-CD45 antibody. Upper panels: CD45 (red); lower panels: merged images of CD45 (red) and DAPI (blue). (D) Number of CD45-positive cells per area. (E) Immunohistochemistry using anti-cleaved caspase 3 antibody across the three inoculation routes. (F) Number of cleaved caspase 3-positive cells per area. (A–F) Control: no virus; NI: nasal inoculation; LI: supra-lingual inoculation; SI: sublingual inoculation. (B, D, F) ****$p < 0.0001$; ***$p < 0.001$; **$p < 0.01$; *$p < 0.05$.

smell may be associated with olfactory sensory neuron infection and can be reproduced in the hamster model following NI.

3.4. SI induced SMG infection with vascular SARS-CoV-2 invasion

We previously reported that angiotensin-converting enzyme 2 is expressed in the ductal epithelium of the mouse SMG [10]. To examine whether SARS-CoV-2 infects the salivary glands, we histologically analyzed SMGs obtained from the control, NI, LI, and SI groups. Inflammatory cell infiltration was observed in all three inoculation groups but not in the control group (Fig. 4A). SARS-CoV-2 was visualized by fluorescent immunohistochemistry, with the strongest signal detected in the ductal epithelium of the SI group (Fig. 4B). Unexpectedly, viral signals were also observed in the lumen near the duct (Fig. 4B, arrowhead), which was histologically confirmed as venous vessels (Fig. 4C, arrowhead). To precisely localize viral signals, fluorescent immunohistochemistry using anti-CD31 and anti–SARS-CoV-2 antibodies was performed in combination with differential interference contrast (DIC) imaging (Fig. 4D and Supplementary Fig. S2A). After coverslip removal, the same sections were subjected to HE staining. Viral signals associated

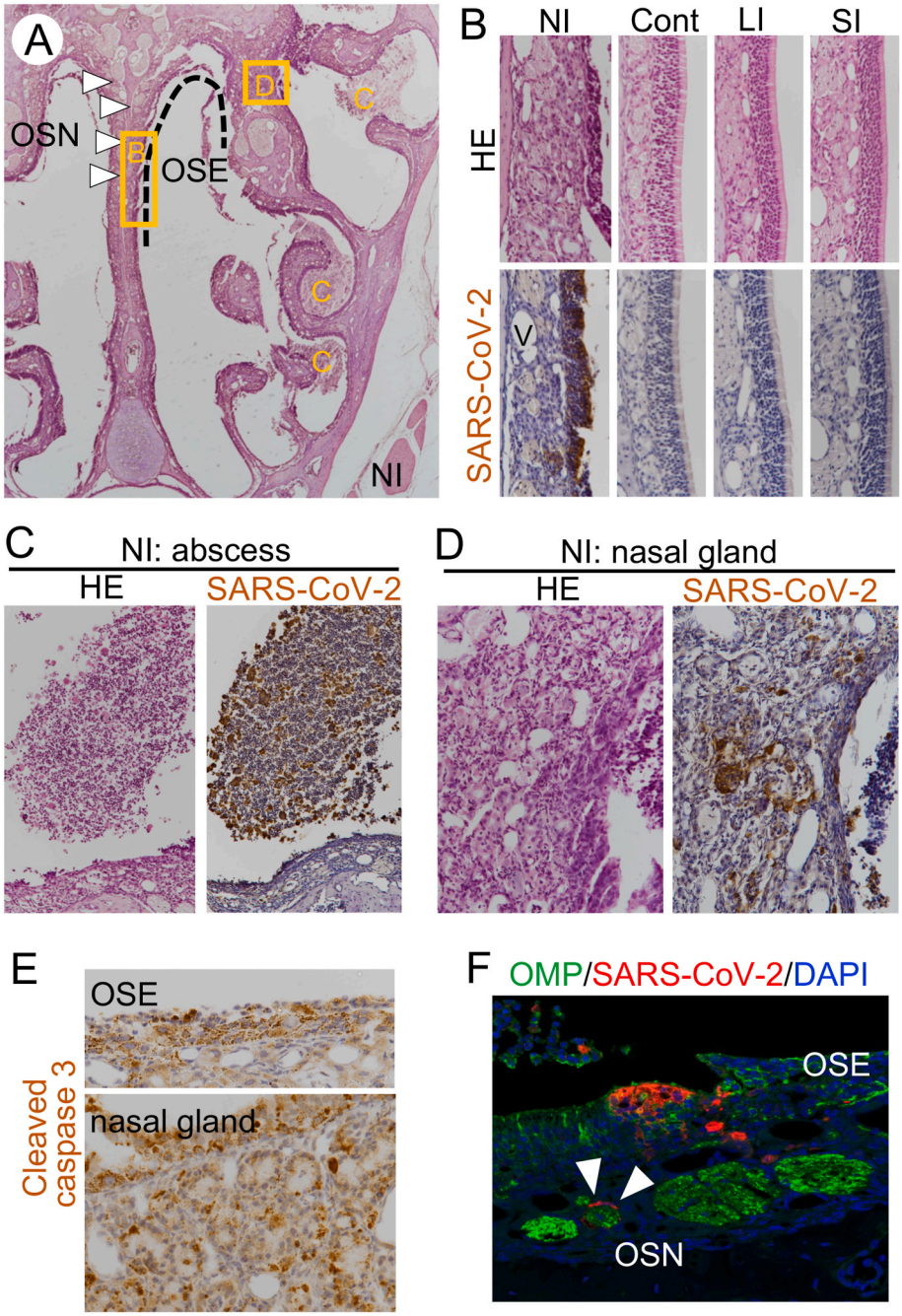

Fig. 3. Severe acute respiratory syndrome coronavirus 2 (SARS-CoV-2) distribution in the nasal cavity following nasal inoculation.
(A) Overview image of the nasal cavity. White arrowhead: olfactory sensory neuron; broken line: olfactory sensory epithelium (OSE); yellow box B: higher magnification across different inoculation routes shown in panel B; yellow box C: abscess shown in panel C; yellow box D: higher magnification shown in panel D. (B) Immunohistochemical detection of SARS-CoV-2 in the OSE across different inoculation routes. Upper panels: hematoxylin–eosin (HE); lower panels: immunohistochemistry; V: vessel. SARS-CoV-2 signal is undetectable. (C) Immunohistochemical detection of SARS-CoV-2 in an abscess following nasal inoculation (NI). Left image: HE; right image: immunohistochemistry. (D) Immunohistochemical detection of SARS-CoV-2 in the nasal glands following NI. Left image: HE; right image: immunohistochemistry. (E) Immunohistochemical detection of cleaved caspase 3 in both the OSE (upper) and nasal glands (lower) following NI. (F) Double immunofluorescence using anti-olfactory marker protein antibody and anti-SARS-CoV-2 antibody (red), with DAPI counterstain (blue).

with blood vessels were localized to the vascular wall rather than the endothelial layer (white arrowhead in Fig. 4D and Supplementary Fig. S2A). Weak viral signals were also detected in both ducts and acini (white arrow). In addition, CD31-positive signals were observed in ductal structures (yellow arrowhead in Supplementary Fig. S2A), likely reflecting the role of CD31 (PECAM-1) as an adhesion molecule involved in tight junctions that prevent saliva leakage [27]. ACE2 expression in salivary gland vasculature was also confirmed (Supplementary Fig. S2B) [28,29]. Quantification of viral signal in the ductal epithelium of the SMG showed that, although all inoculated groups had increased signal compared with the control group, the SI group had significantly higher levels than the NI and LI groups (Fig. 4E). A significantly greater number of CD45-positive inflammatory cells was also found in the SI group compared with the NI and LI groups (Fig. 4F). Cleaved caspase 3-positive apoptotic salivary duct cells were not observed in any group (Supplementary Fig. S3). Moreover, evaluation of vascular viral signals

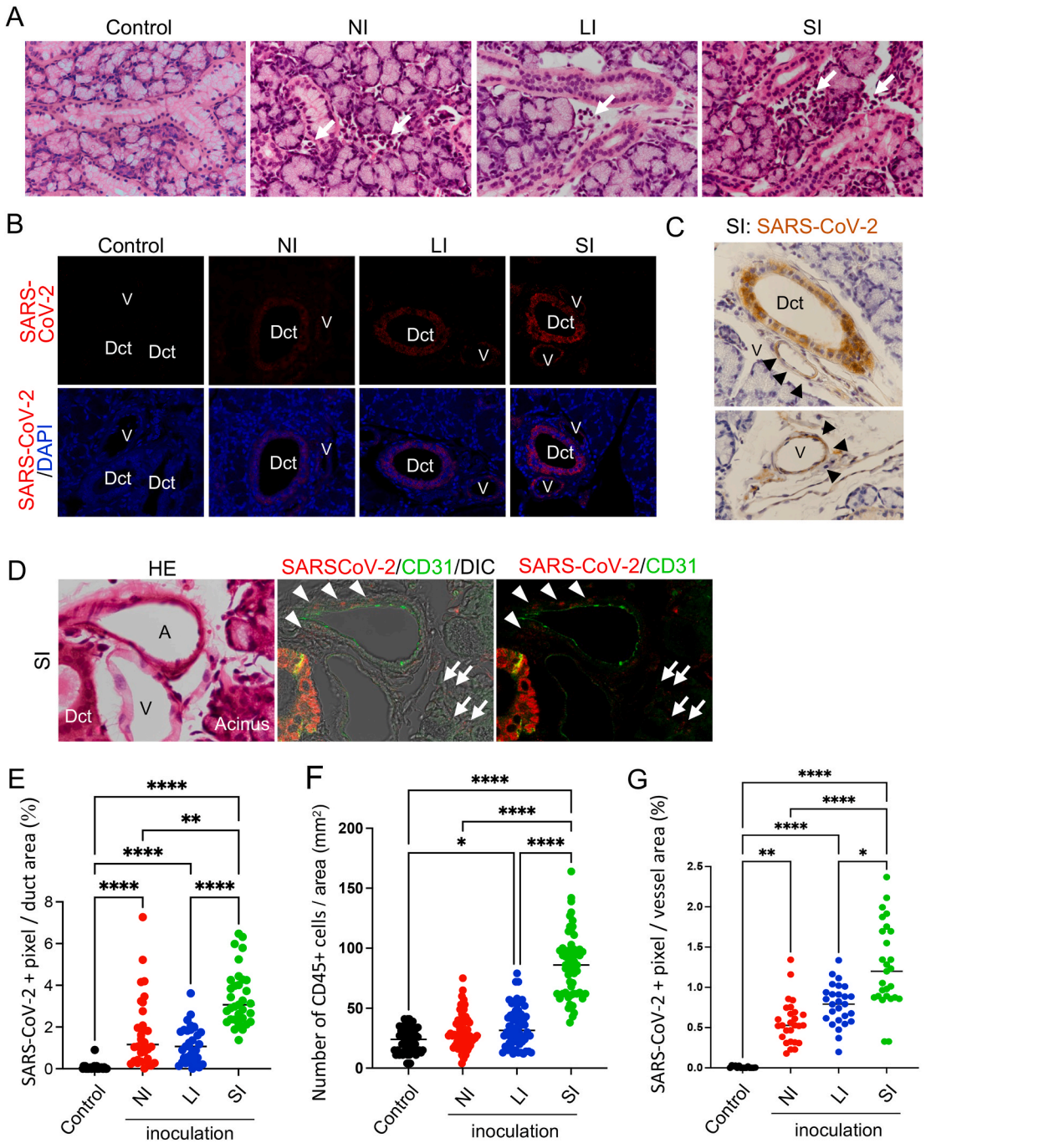

Fig. 4. Comparison of severe acute respiratory syndrome coronavirus 2 (SARS-CoV-2) localization and expression in the submandibular gland (SMG) across different inoculation routes.
(A) Histological images of the SMG across different inoculation routes. (B) Immunofluorescent detection of SARS-CoV-2 in the SMG. Upper panels: SARS-CoV-2 (red); lower panels: merged images of SARS-CoV-2 (red) and DAPI (blue). (C) Immunohistochemical detection of SARS-CoV-2 in the salivary gland duct and vessel in the SI group. Arrowhead: SARS-CoV-2-positive signal in the vessel wall. (D) Immunofluorescence using anti-CD31 antibody (Green) and anti-SARS-CoV-2 antibody (Red) in SARS-CoV-2 sublingual inoculation (SI). White arrowhead: SARS-CoV-2-positive signals in vessel wall, White arrow: SARS-CoV-2-positive signals in acinus. (E) Percentage of SARS-CoV-2-positive area (pixels) in salivary gland ducts across the three inoculation routes. (F) Number of CD45-positive cells per area. (G) Percentage of SARS-CoV-2-positive area (pixels) in SMG vessels across the three inoculation routes. (A–G) Control: no virus; NI: nasal inoculation; LI: supra-lingual inoculation; SI: sublingual inoculation. (B–D) HE: hematoxylin and eosin staining; DIC: Differential interference contrast image; Dct: salivary gland duct; V: venous vessel; A: Arterial vessel. (D–F) ****$p < 0.0001$; **$p < 0.01$; *$p < 0.05$.

revealed that the SI group showed significantly higher levels than both the NI and LI groups (Fig. 4G).

3.5. Comparison of lung delivery across three inoculation routes

Although the NI group showed the highest viral signal in the lungs, CD45-positive inflammatory cells were present in all three inoculation groups (Fig. 1E and 2D). Based on these findings, we hypothesized that the inflammatory cells observed in the lungs of the LI and SI groups resulted from indirect effects of viral infection rather than direct viral entry. To investigate whether the virus might directly reach the lungs through the three inoculation routes, we administered an India

ink–phosphate-buffered saline solution in place of virus and analyzed lung distribution after tissue clearing. The extent of India ink deposition was greatest in the LI group and was scarcely observed in the NI and SI groups (Fig. 5A and B).

3.6. Comparison of liver and brain responses across three inoculation routes

Finally, we performed histological analyses to compare the systemic effects of the three inoculation routes on the liver and brain. Although SARS-CoV-2 was not immunohistochemically detected in the liver (Fig. 6A), CD45-positive immune cell infiltration was observed in the portal areas of the NI and SI groups, but was minimal in the LI and control groups (Fig. 6B). Notably, hepatocellular injury is frequently observed in patients with SARS-CoV-2 infection, supporting the notion that hepatic inflammation may occur independently of direct viral localization [30,31]. Quantitative comparison of infiltrating immune cells among the three inoculation routes revealed that the NI group exhibited the highest level of immune cell infiltration, which was comparable to that observed in the SI group, whereas the LI group showed significantly lower infiltration (Fig. 6C).

In the brain, no SARS-CoV-2 signals were detected (data not shown). CD45-positive immune cell infiltration was observed only in the NI group (Fig. 6D and E), including infiltration in the meninges (Fig. 6F). Such findings are consistent with reports of aseptic meningitis or meningoencephalitis associated with systemic inflammation following SARS-CoV-2 infection [32,33].

A schematic summary of these findings is provided in Fig. 7A and B.

4. Discussion

The primary route of SARS-CoV-2 transmission is thought to be close contact and respiratory droplets released during coughing, sneezing, breathing, and even normal speech [34]. Accordingly, the nasal and oral cavities are considered major entry sites for infection. In this hamster model, we tested three viral inoculation routes—NI, LI, and SI—which respectively mimic conventional upper respiratory tract infection, exposure during speaking and eating, and salivary gland infection. Our findings showed that even when infection originates in the same region of the upper respiratory tract, the pathological outcomes vary depending on the route of viral entry.

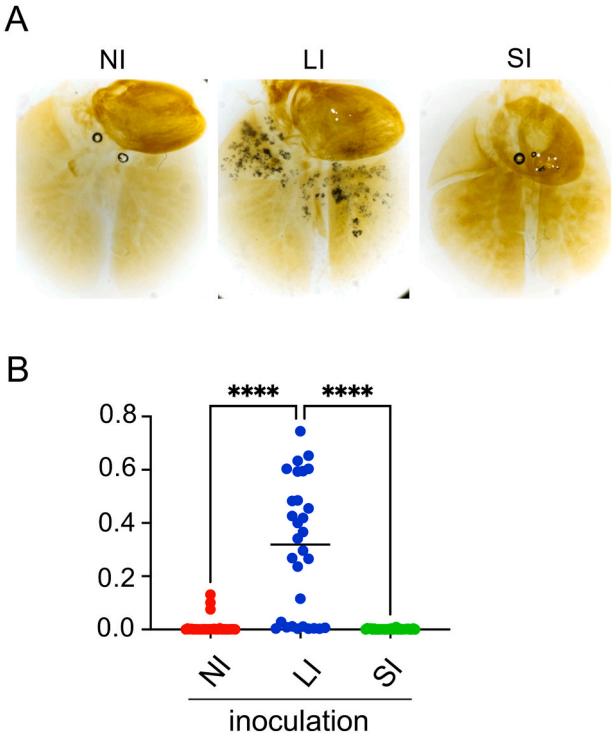

Fig. 5. Lung delivery of India ink via three inoculation routes.
(A) Representative images of lungs after administration of India ink through the three inoculation routes. (B) Percentage of India ink-positive area (pixels) in the lungs following each route. Three hot spots measuring 9000 pixels were selected for each sample, and the percentage of India ink within these regions was calculated. **$p < 0.01$.

In this study, we demonstrated clear differences between the sublingual (SI) and lingual routes (LI) of SARS-CoV-2 infection. Differences between SI and LI were evident in SMG infection: the LI group showed infection at a level comparable to the NI group, whereas the SI group produced significantly higher viral signals in the ductal epithelium of the SMG. In addition, weak viral-positive signals were also observed in acinar cells in the SI group. Previous studies have shown that SARS-CoV-2 can infect the salivary glands including both ductal and acinar components, and viral RNA has been detected in saliva [13]. Furthermore, in a follow-up of 122 hospitalized patients with COVID-19, several exhibited persistent oral symptoms an average of three months after recovery, including salivary gland ectasia (38 %) and xerostomia (30 %) as part of the long COVID syndrome [35]. These findings may reflect ongoing inflammation in the salivary glands.

Although endothelial infection has been described previously, our hamster model showed viral signals predominantly in the vascular wall rather than in CD31-positive endothelial cells. This difference may reflect organ-specific expression of viral entry factors. While ACE2 is expressed in pulmonary endothelial cells, it is mainly detected in pericytes in organs such as the brain, heart, and pancreas [36,37]. Although endothelial infection has been described previously, our hamster model showed viral signals predominantly in the vascular wall rather than in CD31-positive endothelial cells. Although endothelial infection has been described previously, our hamster model showed viral signals predominantly in the vascular wall rather than in CD31-positive endothelial cells [28,29]. In SMG, ACE2 expression was observed not only in endothelial cells but also in cells within the vascular wall. Although the salivary glands and lungs differ in structure and function, both possess dense capillary networks essential for fluid exchange [38,39]. These findings suggest that following SI, the virus may infect the SMG and subsequently access the vasculature via the vascular wall [29]. In contrast, systemic dissemination via the bloodstream warrants further investigation, including quantitative analyses of viral load in blood and more detailed molecular assessments such as PCR-based approaches, in addition to immunohistochemical analyses.

Another important finding is that SARS-CoV-2 inoculated through the nasal cavity (NI) may not directly reach to the lungs but may first infect the nasal mucosa and subsequently spread to the lungs. To replicate severe SARS-CoV-2-induced acute lung injury and acute respiratory distress syndrome in humans, various animal models have been proposed, with nasal administration being the most widely used because of its ability to produce such lesions in the lungs [4,12,20]. However, our replication experiment using India ink–phosphate-buffered saline inoculation through the nasal cavity, which was designed to evaluate the possibility that the virus could reach to the lungs, failed to demonstrate the presence of ink in the lungs. India ink is a mixture of soot and animal glue. Particle size analysis by photon correlation spectroscopy and scanning electron microscopy revealed particle diameters ranging from 130 to 240 nm [40]. These particles are smaller than cough-generated SARS-CoV-2-containing aerosols, which carry the highest viral load at 0.5–100 μm in diameter [41], and they are also smaller than the terminal bronchioles of the Syrian hamster (0.1–0.2 mm in diameter [42]). Our results are consistent with studies of SARS-CoV-2-containing aerosols; Madas et al. speculated that inhalation of cough-generated particles containing SARS-CoV-2 leads primarily to upper airway infection, which can later progress to pneumonia [41]. Our findings are also supported by virological studies showing that even in patients with mild COVID-19,

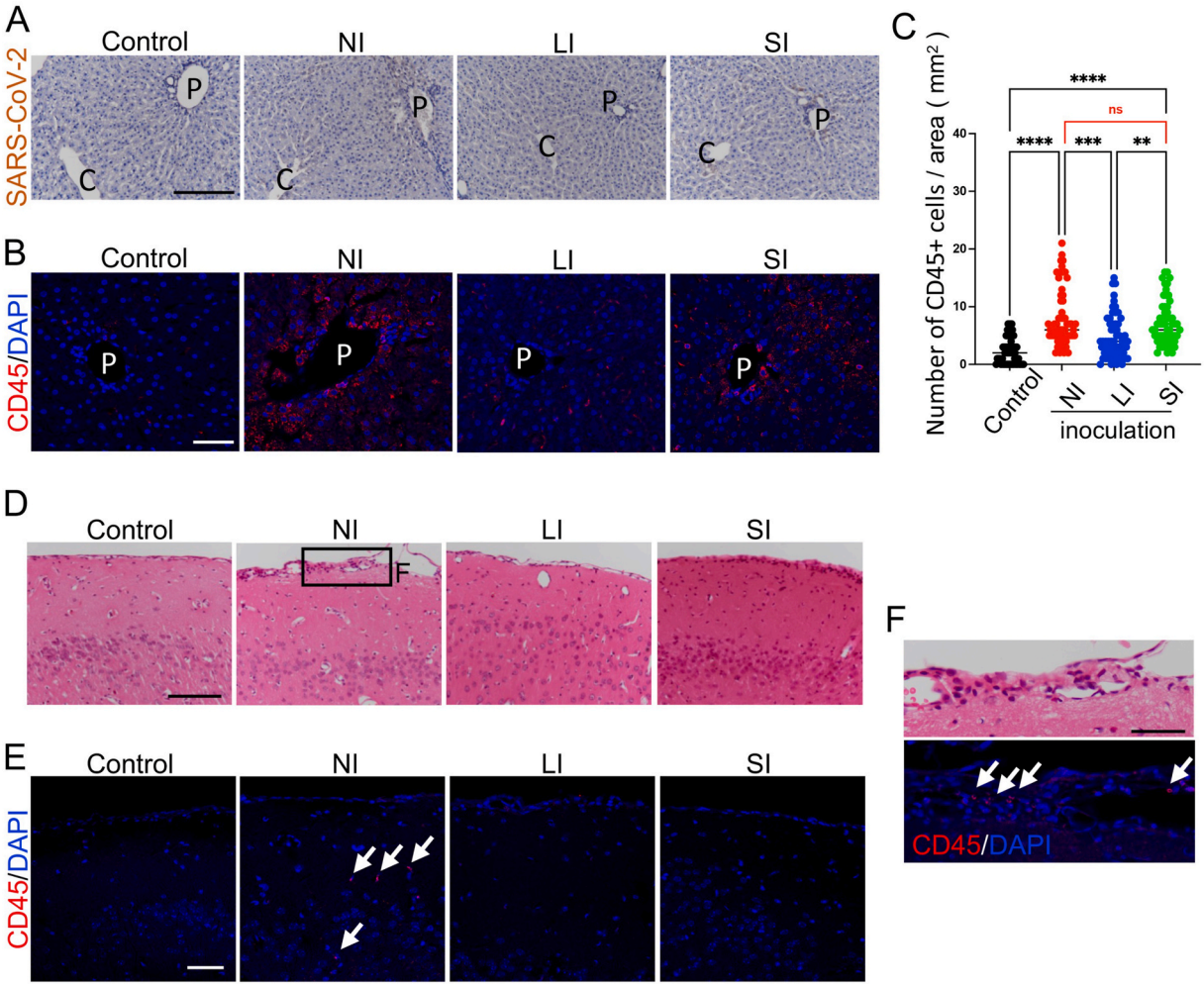

Fig. 6. Liver and brain responses across three inoculation routes
(A) Immunohistochemical detection of SARS-CoV-2 in the liver. Bar = 100 μm. (B) Immunofluorescent detection of CD45-positive immune cell infiltration (red) in the liver. Bar = 50 μm. (A, B) P: portal area; C: hepatic central vein. (C) Number of CD45-positive cells per area. ****$p < 0.0001$; ***$p < 0.001$; **$p < 0.01$; ns: No significant change. (D) Histological images of the brain across different inoculation routes. Representative images of cortical areas with superficial pia mater are shown. Bar = 100 μm. Box in NI: thicken pia mater with immune cell infiltration (higher magnification in F). (E) Immunofluorescent detection of CD45-positive immune cell (red) infiltration in the brain. Bar = 50 μm. Arrow: CD45-positive cells. (F) Higher magnification of box F in (D). Arrow: CD45-positive cells. Bar = 100 μm.

very high concentrations of viral RNA are detectable in early throat swabs [43]. Moreover, clinical studies have reported that some patients with initially mild symptoms experience sudden clinical deterioration approximately one week after symptom onset [2,44]. Together, these experimental and clinical findings suggest that infection and replication in the upper airways are essential for viral spread, and without high viral concentrations in the upper respiratory tract, SARS-CoV-2 would be far less pathogenic.

In our histological analyses, viral signals were detected in the lungs of the NI group, whereas immune cell infiltration was also observed in the lungs of the LI and SI groups. In the liver, immune cell infiltration in the portal areas was observed not only in the NI group, which represents a commonly used infection route [9,11–13], but also in the SI group. These findings suggest the involvement of systemic inflammation, often referred to as a cytokine storm [45,46]. Notably, aseptic meningitis was observed only in the NI group, indicating that the magnitude of systemic cytokine responses may differ depending on the route of infection. Given that cytokines released from the salivary glands can enter the circulation, as reported in Sjögren's syndrome, the SI route and salivary gland infection may also contribute to systemic inflammation [47,48]. However, because circulating viral load and cytokine levels were not directly assessed, further studies are required to clarify systemic viral dissemination and immune responses.

A wide spectrum of clinical manifestations has been reported in SARS-CoV-2 infection [2]. Our analysis suggests that this variability in symptoms may be influenced by the route of viral entry. The infection model developed in this study, which reproduces three possible routes of infection, may provide a valuable tool for understanding the pathophysiology of future emerging infectious diseases transmitted through the upper respiratory tract. Furthermore, the present findings reaffirm that infection prevention measures blocking the viral entry into the oral cavity and upper respiratory tract, such as the use of face masks, are crucial for limiting community spread of upper respiratory tract infections, including SARS-CoV-2.

5. Conclusion

This study demonstrates that the route of viral entry influences both the site and severity of infection. In addition to the well-recognized nasal mucosal route, salivary gland infection may also contribute to systemic viral dissemination. Preventing infections in the upper respiratory tract, including the oral cavity, is therefore likely to be essential. The infection

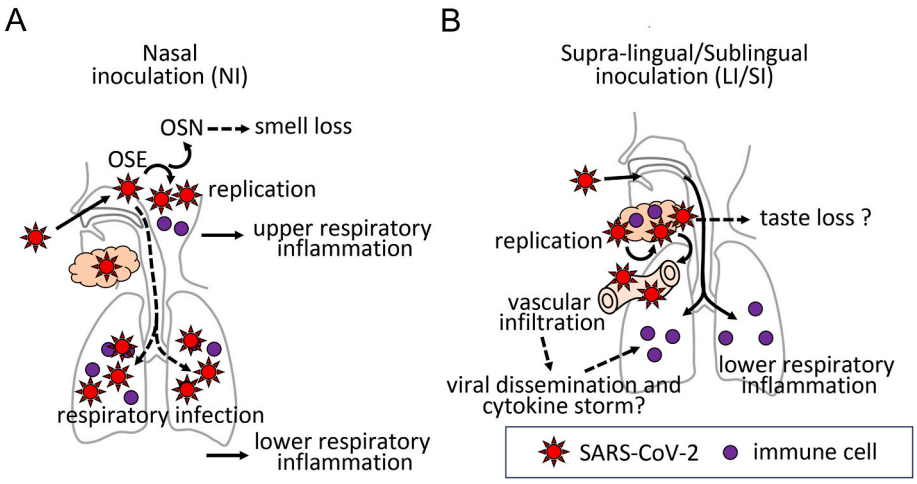

Fig. 7. Schematic summary of the findings.
(A) In the nasal inoculation group, infection was observed in both the olfactory sensory epithelium and the lungs. Infection of the olfactory sensory epithelium and olfactory sensory neurons suggests a mechanism for loss of smell. India ink inoculation via the nasal route suggested that the virus may not directly reach the lungs from the nasal cavity but instead infects the nasal mucosa first, with subsequent replication and secondary spread to the lungs. (B) In the lingual inoculation group, pronounced infection of the submandibular gland was observed, accompanied by vascular involvement, which may suggest an alternative pathway for systemic viral dissemination and cytokine storm. In both the lingual and sublingual groups, histological examination revealed lung inflammation despite the absence of detectable viral antigen, suggesting that oral inoculation routes can induce pulmonary inflammatory responses without direct viral invasion of lung tissue, possibly through cytokine-mediated mechanisms.

model presented here provides a useful tool for analyzing the relationship between transmission routes of pathogenic microorganisms and their pathological consequences, including patterns of dissemination and effects on different organs. This model may also help guide preparedness and decision-making in the event of future zoonotic spillovers.

Ethical approval

All experiments were performed following protocols approved by the Animal Ethics Committee of the Faculty of Dentistry, The University of Osaka (Permit Number: 30-024-0, R-02-009-0) and by the Research Institute for Microbial Diseases, The University of Osaka (Permit Number: R02-17-0).

All experiments involving SARS-CoV-2 were performed in biosafety level-3 (BSL3) laboratory, following the standard biosafety protocols approved by the Research Institute for Microbial Diseases, The University of Osaka (Permit Number: 00137-058).

Contribution statement

NG: Data curation, Formal analysis, Investigation, Visualization. YU: Conceptualization, Data curation, Formal analysis, Funding acquisition, Investigation, Methodology, Visualization, Writing – original draft. KH: Data curation, Investigation. ST: Project administration, Resources, Supervision. SS: Methodology, Resources. TW: Methodology, Resources. CO: Methodology, Resources. TI: Conceptualization, Project administration. TS: Conceptualization, Project administration, Resources, Supervision.

Funding resource

This work was conducted as part of The Nippon Foundation – Osaka University Project for Infectious Disease Prevention (to Y. Usami and T. Sakai). This work was supported by JSPS KAKENHI Grant-in-Aid for Scientific Research (B) (Grant Numbers 19H03852 and 23H030990, to T. Sakai), the Japan Agency for Medical Research and Development (AMED) (Grant Numbers JP223fa627002, to T. Watanabe), the Advanced Research and Development Programs for Medical Innovation (AMED-CREST) (Grant number JP22gm1610010, to T. Watanabe), the Takeda Science Foundation (to T. Watanabe), and the Japan Science and Technology Agency (JST), OPERA Program (Grant Number JPMJOP1861, to T. Inoue).

Declaration competing of interest

The authors declare that they have no known competing financial interests or personal relationships that could have appeared to influence the work reported in this paper.

Acknowledgements

We would like to thank Dr. Tomohiko Takasaki (Kanagawa Prefectural Institute of Public Health) for providing the SARS-CoV-2/Hu/DP/Kng/19–020 strain. We also acknowledge Editage (www.editage.jp) for English language editing.

Appendix A. Supplementary data

Supplementary data to this article can be found online at https://doi.org/10.1016/j.job.2026.100746.

References

[1] Zhu N, Zhang D, Wang W, Li X, Yang B, Song J, et al. A novel coronavirus from patients with pneumonia in China. 2019. N Engl J Med 2020;382:727–33.
[2] Huang C, Wang Y, Li X, Ren L, Zhao J, Hu Y, et al. Clinical features of patients infected with 2019 novel coronavirus in Wuhan, China. Lancet 2020;395:497–506.
[3] de Wit E, van Doremalen N, Falzarano D, Munster VJ. SARS and MERS: recent insights into emerging coronaviruses. Nat Rev Microbiol 2016;14(8):523–34.
[4] Choudhary S, Kanevsky I, Tomlinson L. Animal models for studying COVID-19, prevention, and therapy: pathology and disease phenotypes. Vet Pathol 2022;59:516–27.
[5] Tang S, Mao Y, Jones RM, Tan Q, Ji JS, Li N, et al. Aerosol transmission of SARS-CoV-2? Evidence, prevention and control. Environ Int 2020;144:106039.
[6] Zhang R, Li Y, Zhang AL, Wang Y, Molina MJ. Identifying airborne transmission as the dominant route for the spread of COVID-19. Proc Natl Acad Sci U S A 2020;117(26):14857–63.
[7] Atyeo N, Perez P, Matuck B, Byrd KM, Warner BM. The mouth as a site of SARS-CoV-2 infection. Curr Oral Health Rep 2024;11:167–76.
[8] Sato T, Ueha R, Goto T, Yamauchi A, Kondo K, Yamasoba T. Expression of ACE2 and TMPRSS2 proteins in the upper and lower aerodigestive tracts of rats: implications on COVID 19 infections. Laryngoscope 2021;131(3):E932–9.

[9] Ueha R, Ito T, Furukawa R, Kitabatake M, Ouji-Sageshima N, Ueha S, et al. Oral SARS-CoV-2 inoculation causes nasal viral infection leading to olfactory bulb infection: an experimental study. Front Cell Infect Microbiol 2022;12:924725.
[10] Usami Y, Hirose K, Okumura M, Toyosawa S, Sakai T. Brief communication: immunohistochemical detection of ACE2 in human salivary gland. Oral Sci Int 2021;18(2):101–4.
[11] Lee AC, Zhang AJ, Chan JF, Li C, Fan Z, Liu F, et al. Oral SARS-CoV-2 inoculation establishes subclinical respiratory infection with virus shedding in golden Syrian hamsters. Cell Rep Med 2020;1(7):100121.
[12] Bi Z, Hong W, Yang J, Lu S, Peng X. Animal models for SARS-CoV-2 infection and pathology. MedComm 2021;2(4):548–68.
[13] Huang N, Pérez P, Kato T, Mikami Y, Okuda K, Gilmore RC, et al. SARS-CoV-2 infection of the oral cavity and saliva. Nat Med 2021;27(5):892–903.
[14] Schneider C, Rasband W, Eliceiri K. NIH Image to ImageJ: 25 years of image analysis. Nat Methods 2012;9:671–5.
[15] van den Brand JM, Stittelaar KJ, van Amerongen G, Rimmelzwaan GF, Simon J, de Wit E, et al. Severity of pneumonia due to new H1N1 influenza virus in ferrets is intermediate between that due to seasonal H1N1 virus and highly pathogenic avian influenza H5N1 virus. J Infect Dis 2010;201(7):993–9.
[16] Haagmans BL, Kuiken T, Martina BE, Fouchier RA, Rimmelzwaan GF, van Amerongen G, et al. Pegylated interferon-alpha protects type 1 pneumocytes against SARS coronavirus infection in macaques. Nat Med 2004;10(3):290–3.
[17] Araie T, Ono Minagi H, Usami Y, Ikai K, Sakai M, Gojo N, et al. Effect of xanthan gum-thickened liquid aspiration on the lung in a mouse model. Oral Sci Int 2020;17(2):78–85.
[18] Shirogane Y, Usami Y, Okumura M, Hirose K, Naniwa K, Ikebe K, et al. Anti-VEGFR2 neutralising antibody slows the progression of multistep oral carcinogenesis. J Pathol 2024;264(4):423–33.
[19] Essalmani R, Jain J, Susan-Resiga D, Andréo U, Evagelidis A, Derbali RM, et al. Distinctive roles of Furin and TMPRSS2 in SARS-CoV-2 infectivity. J Virol 2022;96(8):e0012822.
[20] Gruber AD, Firsching TC, Trimpert J, Dietert K. Hamster models of COVID-19 pneumonia reviewed: how human can they be? Vet Pathol 2022;59(4):528–45.
[21] Choudhary S, Kanevsky I, Tomlinson L. Animal models for studying COVID-19, prevention, and therapy: pathology and disease phenotypes. Vet Pathol 2022;59(4):516–27.
[22] Yuan C, Ma Z, Xie J, Li W, Su L, Zhang G, et al. The role of cell death in SARS-CoV-2 infection. Signal Transduct Target Ther 2023;8(1):357.
[23] Liu Y, Garron TM, Chang Q, Su Z, Zhou C, Qiu Y, et al. Cell-Type apoptosis in lung during SARS-CoV-2 infection. Pathogens 2021;10(5):509.
[24] Khan M, Yoo SJ, Clijsters M, Backaert W, Vanstapel A, Speleman K, et al. Visualizing in deceased COVID-19 patients how SARS-CoV-2 attacks the respiratory and olfactory mucosae but spares the olfactory bulb. Cell 2021;184(24):5932–49.
[25] Chen M, Pekosz A, Villano JS, Shen W, Zhou R, Kulaga H, et al. Evolution of nasal and olfactory infection characteristics of SARS-CoV-2 variants. J Clin Investig 2024;134(8):e174439.
[26] Barrios AW, Núñez G, Sánchez Quinteiro P, Salazar I. Anatomy, histochemistry, and immunohistochemistry of the olfactory subsystems in mice. Front Neuroanat 2014;8:63.
[27] Hata M, Ueki T, Sato A, Kojima H, Sawa Y. Expression of podoplanin in the mouse salivary glands. Arch Oral Biol 2008;53(9):835–41.
[28] Muhl L, He L, Sun Y, Andaloussi Mäe M, Pietilä R, Liu J, et al. The SARS-CoV-2 receptor ACE2 is expressed in mouse pericytes but not endothelial cells: implications for COVID-19 vascular research. Stem Cell Rep 2022;17(5):1089–104.
[29] Martínez-Salazar B, Holwerda M, Stüdle C, Piragyte I, Mercader N, Engelhardt B, et al. COVID-19 and the vasculature: current aspects and long-term consequences. Front Cell Dev Biol 2022;10:824851.
[30] Phipps MM, Barraza LH, LaSota ED, Sobieszczyk ME, Pereira MR, Zheng EX, et al. Acute liver injury in COVID-19: prevalence and association with clinical outcomes in a large U.S. cohort. Hepatology 2020;72(3):807–17.
[31] Marjot T, Webb GJ, Barritt AS, Moon AM, Stamataki Z, Wong VW, et al. COVID-19 and liver disease: mechanistic and clinical perspectives. Nat Rev Gastroenterol Hepatol 2021;18(5):348–64.
[32] Lv P, Peng F, Zhang Y, Zhang L, Li N, Sun L, et al. COVID-19-associated meningoencephalitis: a care report and literature review. Exp Ther Med 2021;21(4):362.
[33] Cergole-Novella MC, Bispo TR, Matsuda EM, Colpas DR, Campos IB. SARS-CoV-2 investigation in cerebrospinal fluid from meningitis patients during the first pandemic wave. Braz J Infect Dis 2025;29(5):104571.
[34] Falahi S, Kenarkoohi A. Transmission routes for SARS-CoV-2 infection: review of evidence. New Microbes New Infect 2020;38:100778.
[35] Gherlone EF, Polizzi E, Teté G, De Lorenzo R, Magnaghi C, Rovere Querini P, et al. Frequent and persistent salivary gland ectasia and oral disease after COVID-19. J Dent Res 2021;100(5):464–71.
[36] Varga Z, Flammer AJ, Steiger P, Haberecker M, Andermatt R, Zinkernagel AS, et al. Endothelial cell infection and endotheliitis in COVID-19. Lancet 2020;395(10234):1417–8.
[37] Ackermann M, Verleden SE, Kuehnel M, Haverich A, Welte T, Laenger F, et al. Pulmonary vascular endothelialitis, thrombosis, and angiogenesis in Covid-19. N Engl J Med 2020;383(2):120–8.
[38] Ohtani O, Ohtsuka A, Lipsett J, Gannon B. The microvasculature of rat salivary glands. A scanning electron microscopic study. Acta Anat 1983;115(4):345–56.
[39] Miller CS, Foley JD, Bailey AL, Campell CL, Humphries RL, Christodoulides N, et al. Current developments in salivary diagnostics. Biomark Med 2010;4(1):171–89.
[40] Swider JR, Hackley VA, Winter J. Characterization of Chinese ink in size and surface. J Cult Herit 2003;4(3):175–86.
[41] Madas BG, Füri P, Farkas Á, Nagy A, Czitrovszky A, Balásházy I, et al. Deposition distribution of the new coronavirus (SARS-CoV-2) in the human airways upon exposure to cough-generated droplets and aerosol particles. Sci Rep 2020;10(1):22430.
[42] Kennedy AR, Desrosiers A, Terzaghi M, Little JB. Morphometric and histological analysis of the lungs of Syrian golden hamsters. J Anat 1978;125(Pt 3):527–53.
[43] Wölfel R, Corman VM, Guggemos W, Seilmaier M, Zange S, Müller MA, et al. Virological assessment of hospitalized patients with COVID-2019. Nature 2020;581(7809):465–9.
[44] Wu C, Chen X, Cai Y, Xia J, Zhou X, Xu S, et al. Risk factors associated with acute respiratory distress syndrome and death in patients with coronavirus disease 2019 pneumonia in Wuhan, China. JAMA Intern Med 2020;180(7):934–43.
[45] Elshazli RM, Toraih EA, Elgaml A, El-Mowafy M, El-Mesery M, Amin MN, et al. Diagnostic and prognostic value of hematological and immunological markers in COVID-19 infection: a meta-analysis of 6320 patients. PLoS One 2020;15(8):e0238160.
[46] Jamalidoust M, Hamzavi SS, Shorafa E, Namayandeh M, Batool L, Abootalebi SN. Comparing clinical presentation, viremia, and immunological factors at various severity presentations in hospitalized children affected by COVID-19: a cross-sectional study. Health Sci Rep 2023;6(5):e1259.
[47] Katsifis GE, Rekka S, Moutsopoulos NM, Pillemer S, Wahl SM. Systemic and local interleukin-17 and linked cytokines associated with Sjögren's syndrome immunopathogenesis. Am J Pathol 2009;175(3):1167–77.
[48] Dong Y, Wang T, Wu H. The role of cytokines from salivary gland epithelial cells in the immunopathology of Sjögren's syndrome. Front Immunol 2024;15:1443455.